LETTER

doi:10.1038/nature11619

Linking synchronization to self-assembly using magnetic Janus colloids

Jing Yan[1], Moses Bloom[2], Sung Chul Bae[1], Erik Luijten[2,3] & Steve Granick[1,4,5]

Synchronization occurs widely in the natural and technological worlds, from the rhythm of applause and neuron firing[1] to the quantum mechanics of coupled Josephson junctions[2], but has not been used to produce new spatial structures. Our understanding of self-assembly has evolved independently in the fields of chemistry and materials, and with a few notable exceptions[3,4] has focused on equilibrium rather than dynamical systems. Here we combine these two phenomena to create synchronization-selected microtubes of Janus colloids, micron-sized spherical particles with different surface chemistry on their opposing hemispheres, which we study using imaging and computer simulation. A thin nickel film coats one hemisphere of each silica particle to generate a discoid magnetic symmetry, such that in a precessing magnetic field its dynamics retain crucial phase freedom. Synchronizing their motion, these Janus spheres self-organize into micrometre-scale tubes in which the constituent particles rotate and oscillate continuously. In addition, the microtube must be tidally locked to the particles, that is, the particles must maintain their orientation within the rotating microtube. This requirement leads to a synchronization-induced structural transition that offers various applications based on the potential to form, disintegrate and fine-tune self-assembled in-motion structures *in situ*. Furthermore, it offers a generalizable method of controlling structure using dynamic synchronization criteria rather than static energy minimization, and of designing new field-driven microscale devices in which components do not slavishly follow the external field.

Consider applause after a musical performance[5]. After a short period of chaotic clapping, applause often becomes rhythmic—everyone claps with the same phase and tempo. This illustrates fundamental elements of synchronization: the individual units display periodic motion, they display adjustable phase and frequency, and they couple[6]. However, in such classic synchronization problems units lack the freedom to change position in response to their interaction, a spatial adaptability that is essential to self-assembly. Here we considered situations where synchronization and self-assembly are inextricably linked and led to a new type of colloidal assembly. As proof of concept, we examined the example of magnetic Janus spheres.

Thin nickel films (18 nm or 21 nm) were directionally deposited onto one hemisphere of 3-μm spherical silica particles[7,8]. The magnetic response of these particles is smaller along the Janus director (red arrow in Fig. 1a) and larger in the plane perpendicular to it (Supplementary Fig. 2), yielding a discoid symmetry. Suspended in deionized water, the spheres sedimented close to the chamber bottom. In optical images they appeared like the phases of the moon, owing to the dark metal coating. By applying a precessing magnetic field[9–11] (Fig. 1a), we produced a torque on each sphere with two orthogonal components, one that drove it to spin around the precession axis with angle φ, and another that drove it to oscillate perpendicular to the rotating plane with angle α (Supplementary Fig. 4 and Supplementary Videos 1 and 2). The resulting dynamics, which resembled a gyroscope's nutation, are quantitatively captured by the equations of motion (Methods). Notably, the rotation and oscillation frequencies can be controlled by the precession angle θ (Fig. 1b).

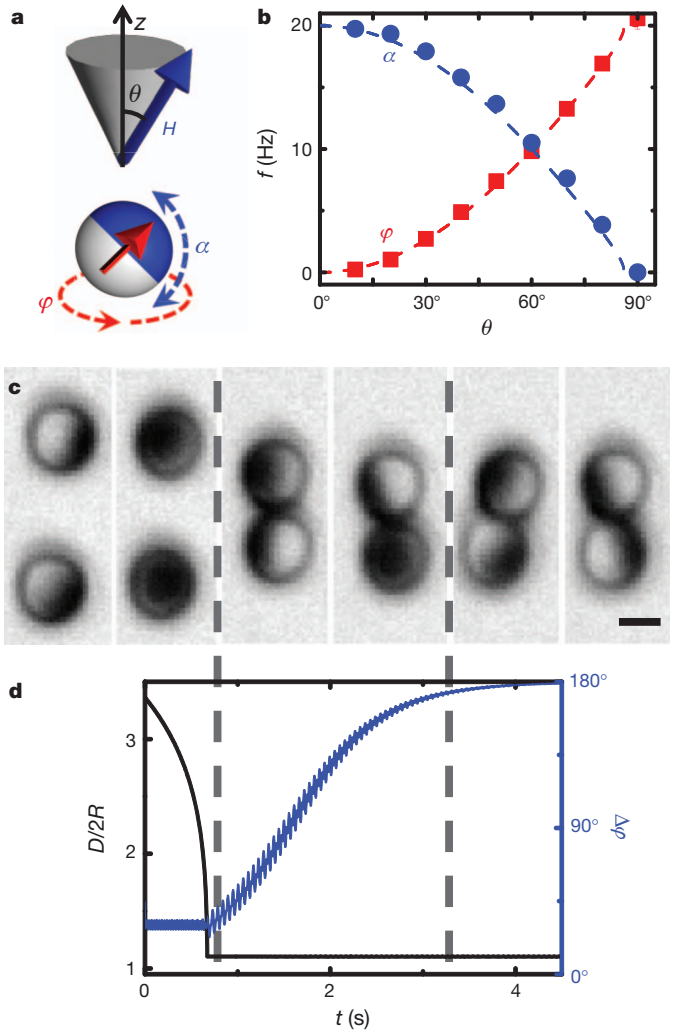

Figure 1 | Single- and two-particle dynamics in precessing fields. **a**, Janus director (red) rotates around precession axis z (angle φ) while oscillating perpendicularly (angle α), in a precessing field H with precession angle θ. **b**, Measured frequencies of φ and α versus θ confirm predictions (dashed lines). Nickel coating, 18 nm. **c**, Images of two approaching particles at $\theta = 25°$ (precession axis is vertical) at successive times. Initially approximately in-phase, the directors end in anti-phase (scale bar, 2 μm). **d**, Centre-to-centre separation D (normalized by diameter $2R$) and phase difference $\Delta\varphi$ versus time t from simulations under the same conditions. After the separation reaches its minimum, $\Delta\varphi$ gradually approaches its steady-state value 180°. Vertical dashed lines mark corresponding parts of panels **c** and **d**.

[1]Department of Materials Science and Engineering, University of Illinois, Urbana, Illinois 61801, USA. [2]Department of Materials Science and Engineering, Northwestern University, Evanston, Illinois 60208, USA. [3]Department of Engineering Sciences and Applied Mathematics, Northwestern University, Evanston, Illinois 60208, USA. [4]Department of Physics, University of Illinois, Urbana, Illinois 61801, USA. [5]Department of Chemistry, University of Illinois, Urbana, Illinois 61801, USA.

©2012 Macmillan Publishers Limited. All rights reserved

Hence, for most experiments we employed a fixed frequency f (20 Hz) and field strength (5 mT), leaving θ as the control parameter. Although composed of Brownian particles, the system was deterministic, with interactions around 10^4 times the thermal energy. Therefore, our findings could in principle scale up to macroscopic systems.

Phase freedom[12], a consequence of the discoid magnetic symmetry, allows interacting spheres to adjust their phases. For example, two particles (Fig. 1c) initially attract and approach until stopped by electrostatic repulsion at a separation of about 200 nm. Only at this close separation does the magnetic field created by one particle generate an appreciable torque on the other particle. Although small, this torque gradually drove the two particles to an antiphase steady state in both α and φ, regardless of the initial state. Once synchronized, the particles' rotation slowed slightly, while their geometric centres started to rotate around a common central axis. Their spatial positions are staggered head-to-tail owing to the Janus feature, which is captured in simulation by a point dipole moment shifted from the particle's geometric centre[13]. We observed frequency locking even when particles had different coating thicknesses and hence different inherent frequencies.

Next we considered suspensions of these Janus spheres. At low precession angle θ, we observed a family of long, defect-free microtubes forming spontaneously (region I in Fig. 2a). Structurally, unlike the chiral helices observed in amphiphilic self-assembly[14] or magnetic assembly directed by steric hindrance[15], these microtubes were achiral and can be interpreted as staggered stacks of regular polygons with k edges (Fig. 2b). We labelled them (kk0), following classic nomenclature[16]. Their formation followed a nucleation-and-growth scheme (Supplementary Video 5). Initially, zigzag chains approached and wrapped around one another randomly, then short ordered (kk0) strands nucleated, and finally nuclei propagated to 'zip up' a corresponding structure. Once formed, these structures rolled on the substrate. Within region I of the dynamic state diagram, the distribution of microtubes changed with θ (Fig. 2c): increasing θ shifted the distribution towards smaller k. On exceeding a threshold θ only zigzag chains were observed (region II) and subsequent increase of θ transformed them in known ways[9,11] into hexagonal sheets oriented perpendicular to the precession axis (region III, Fig. 2d). The synchronization-induced structural transitions of interest here occurred at relatively low θ where the frequency dependence is small.

Although static tubular packings have long been known[16] and realized recently[17], here the spheres remained in continual motion, exhibiting nutation-like dynamics even within the aggregate. Moreover, they synchronized: for example, Supplementary Video 7 shows three particles within a triangular cross-section of the (330) structure, locked into a 120° phase shift (Fig. 3a).

The most striking synchronization occurred between the rotating microtube and its constituent particles, such that the spheres' metallic faces continually faced inward, reminiscent of the familiar tidal locking of the Moon and Earth. This dynamic requirement is the key to understanding the structural stability. We analysed this system ignoring interactions between microtubes, which is a valid assumption for a broad range of volume fractions. We considered a (330) structure in its lowest-energy configuration in a static field, with each sphere's director pointing to the central axis. Once the precessing field was switched on, the constituent particles rotated with respect to the tube and adopted an average orientation that deviates from inward-pointing by an angle ψ defined in Fig. 3b. Distorting the lowest-energy configuration, this generated a restoring torque $\mathrm{d}E/\mathrm{d}\psi$ (incorporating all many-body interactions) that rotated the tube while slowing the constituent particles. It was proportional to $\sin\psi$ (Supplementary Fig. 9) with a proportionality coefficient ε that quantifies rotational coupling between the tube and particle and depends on the instantaneous tube configuration. Balancing this magnetic torque with viscous drag, we find (see Supplementary Information for the derivation):

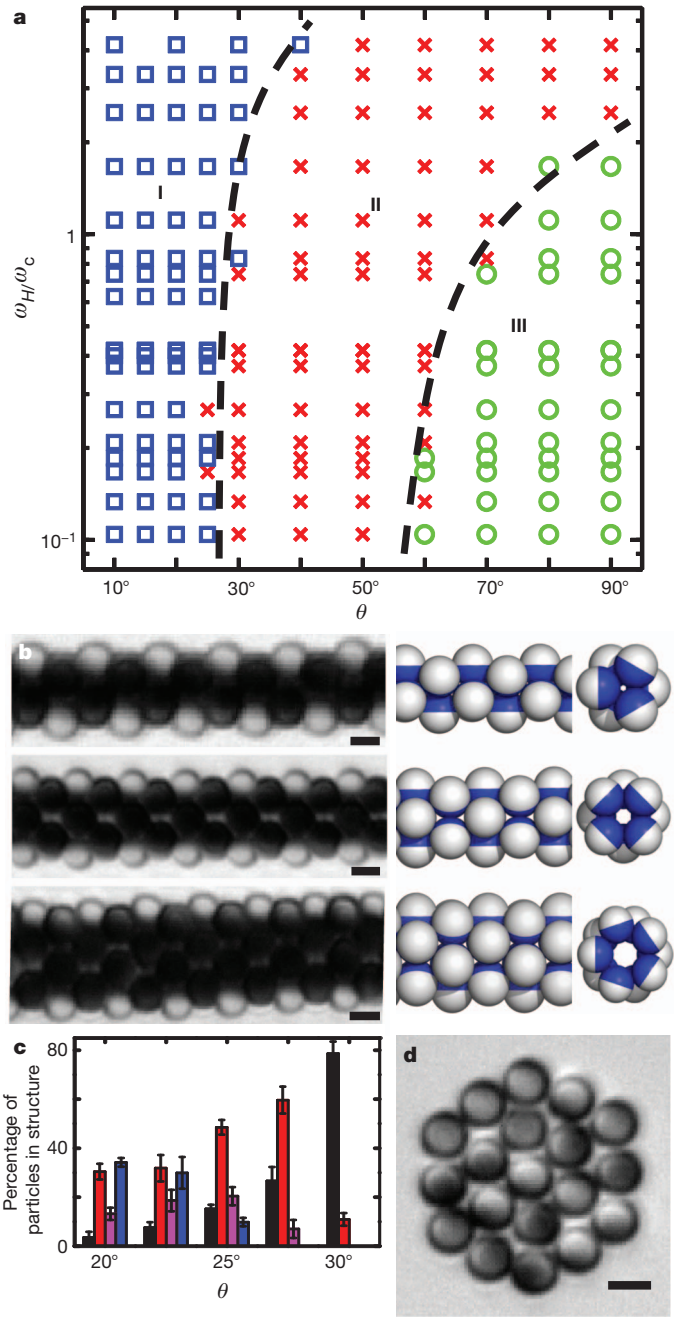

Figure 2 | Synchronized self-assembly. a, Measured dynamic state diagram in the ω_H–θ plane. The external field frequency ω_H is normalized by the characteristic frequency ω_c (Methods). Boundaries (black lines) are guides to the eye. Regions I, II and III involve microtubes, zigzag chains and planar sheets, respectively. **b**, Observed images (left) and corresponding models (right, side and end views) of microtubes (k = 3, 4, 5) parallel to the precession axis. **c**, Dependence on θ of the distribution of microtubes. Nickel coating, 21 nm. (550), blue; (440), magenta; (330), red; zigzag chain, black. Error bars correspond to one standard deviation. Results are obtained from four independent samples each containing more than 3,000 particles. **d**, Hexagonal sheets perpendicular to the precession axis in region III ($\theta = 70°$). All scale bars are 3 μm.

$$\frac{\mathrm{d}\psi}{\mathrm{d}t} = \omega_{\mathrm{free}} - \varepsilon(\zeta_{\mathrm{r}}^{-1} + \zeta_{\mathrm{tube}}^{-1})\sin\psi \qquad (1)$$

Here ω_{free} is the angular velocity of free particles under the same condition, and ζ_{r} and ζ_{tube} are the rotational friction coefficients of the single particle and the entire tube, respectively. Although in principle the hydrodynamic forces[18,19] should matter, their effect is secondary to

©2012 Macmillan Publishers Limited. All rights reserved

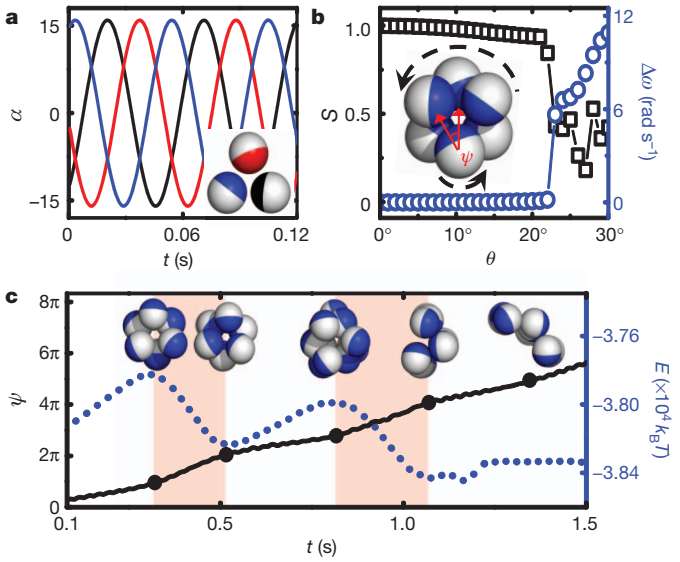

Figure 3 | Synchronization-induced structural transitions. **a**, Illustration of phase locking of the oscillation angle α for cross-sectional particles in a (330) microtube (inset), simulated at $\theta = 18^\circ$. **b**, Order parameter S and difference $\Delta\omega$ in rotation frequency between constituent particle and microtube, plotted versus θ for simulated (330) microtube (inset). Particle directors deviate from centre-pointing by angle ψ. Arrows indicate rotation of tube and individual sphere. **c**, Time evolution of ψ (black) and energy E (blue) during disassembly of an unstable (330) microtube at $\theta = 30^\circ$. Shaded regions highlight phase slip. Snapshots (inset models) along the time axis are shown at times indicated by dots.

the magnetic forces (Supplementary Information). Equation (1) has the same mathematical form as the classical Adler equation for synchronization[20], so we can apply all the general analyses of this equation.

A crucial prediction of equation (1) is the existence of a critical frequency above which an assembly cannot track its constituent particles. If $\omega_{\mathrm{free}} > \varepsilon(\zeta_{\mathrm{r}}^{-1} + \zeta_{\mathrm{tube}}^{-1})$, no steady-state solution (that is, $\mathrm{d}\psi/\mathrm{d}t = 0$) exists. In that case, the time trajectory of ψ displays periodic phase slips[21] (shaded regions in Fig. 3c), leading to a transient high-energy configuration where the magnetic hemispheres of constituent particles face outward. This unsynchronized state ultimately dissociated into a loose aggregate of zigzag chains with lower average energy. Because ω_{free} depends monotonically on θ, a critical ω_{free} translates into a critical θ_{c}. Figure 3b confirms the coupling between the loss of synchronization, characterized by the difference $\Delta\omega$ in rotational frequency of the constituent particles and the entire structure, and the structural transition, reflected by the sharp decrease of the positional order parameter S (defined in Methods). This process explains the boundary between regions I and II of Fig. 2a.

This dynamics-induced transition offers interesting possibilities for structural selection (Fig. 2c) that would not be possible with conventional static energy minimization. The large energy barriers between different ($kk0$) tubes preclude thermal equilibration and hence both in static fields and at low θ a broad distribution of k was observed. However, at higher θ, synchronization criteria set in. The larger the tube diameter, the smaller the coupling strength ε and the larger the friction ζ_{tube}, leading to lower dissociation angle θ_{c}. For example, with increasing θ in Fig. 2c we saw fewer (550) microtubes and none above θ_{c} (which is about 25° for this structure). The abundance of medium-diameter structures such as (330) thus first increased at the expense of thicker structures and dominated at some angles. This agrees qualitatively with the trend seen in simulation (Supplementary Fig. 13).

Modulation of the magnetic properties allows other types of tubular packing as well. Consistent with simulations from random initial conditions, we also observed ($kk2k$) and chiral structures when we coated the same nickel films onto paramagnetic spheres (Supplementary Video 9). Such particles are indeed closer to the shifted-dipole model used in simulation, because their magnetic properties are dominated by the bulk rather than the thin film coating, whose magnetic properties are complicated by the coating profile[22].

On the basis of their capacity for *in situ* assembly, disassembly and reconfigurability, the structures demonstrated in this study suggest various potential applications, such as selective cargo uptake and transport[23] inside these hollow microtubes and fluid flow control[24] with the known high efficiency of synchronized states[6,19,24]. The path is also clear to extend these approaches using patterned arrays of external driving sources[25] to achieve spatially resolved reconfigurable structures.

These synchronization criteria suggest a materials selection method complementary to the conventional equilibrium approach of energy minimization. To dynamically destabilize structures that compete with targeted ones could benefit the current trend of designing self-assembly of anisotropic building blocks[26–28] (which tend to form multiple possible structures), and may stimulate related consideration of other dynamical systems, both smaller (molecular) and larger (granular) than considered here. This argument applies generally to magnetic, electric, chemical and hydrodynamic fields. The required phase-free dynamics can be achieved by designing shapes more complex than the simple spheres considered here or more generally via a driving frequency so high that building blocks cannot track the field. Such non-slaved responses to external fields have been underappreciated in self-assembly but are shown here to result in structures impossible with classical slaved motion[3,4,29,30].

METHODS SUMMARY

Nickel coatings of 18 nm or 21 nm followed by 15–20 nm SiO_2 are deposited vertically onto a planar submonolayer of monodisperse 3-μm silica particles using electron-beam deposition. The particles are washed thoroughly with deionized water and isopropyl alcohol, then sonicated and collected in deionized water. A spatially homogeneous precessing magnetic field generated by three orthogonal pairs of solenoids is applied within a home-built microscope equipped with a 50× long-working-distance objective and a complementary metal–oxide–semiconductor camera. Particle tracking is performed using Matlab with home-written code. Molecular dynamics simulations are performed using spherical particles with excluded-volume interactions (represented by a shifted-truncated Lennard–Jones potential) and magnetic dipole moments computed self-consistently every time step. Magnetic parameters are chosen in accordance with experiment. Simulations involve up to 80 particles and cover 2×10^8 time steps, corresponding to 25.2 s in experiment; doubling the system size confirms the same trends.

Full Methods and any associated references are available in the online version of the paper.

Received 1 June; accepted 25 September 2012.

1. Strogatz, S. *Sync: the Emerging Science of Spontaneous Order* Ch. 2 (Hyperion, 2003).
2. Ozyuzer, L. *et al.* Emission of coherent THz radiation from superconductors. *Science* **318,** 1291–1293 (2007).
3. Grzybowski, B. A., Stone, H. A. & Whitesides, G. M. Dynamic self-assembly of magnetized, millimetre-sized objects rotating at a liquid–air interface. *Nature* **405,** 1033–1036 (2000).
4. Snezhko, A. & Aranson, I. S. Magnetic manipulation of self-assembled colloidal asters. *Nature Mater.* **10,** 698–703 (2011).
5. Néda, Z., Ravasz, E., Brechet, Y., Vicsek, T. & Barabási, A.-L. The sound of many hands clapping. *Nature* **403,** 849–850 (2000).
6. Pikovsky, A., Rosenblum, M. & Kurths, J. *Synchronization: a Universal Concept in Nonlinear Sciences* (Cambridge, 2001).
7. Sinn, I. *et al.* Magnetically uniform and tunable Janus particles. *Appl. Phys. Lett.* **98,** 024101 (2011).
8. Smoukov, S. K., Gangwal, S., Marquez, M. & Velev, O. D. Reconfigurable responsive structures assembled from magnetic Janus particles. *Soft Matter* **5,** 1285–1292 (2009).
9. Osterman, N. *et al.* Field-induced self-assembly of suspended colloidal membranes. *Phys. Rev. Lett.* **103,** 228301 (2009).
10. Tierno, P., Claret, J., Sagués, F. & Cēbers, A. Overdamped dynamics of paramagnetic ellipsoids in a precessing magnetic field. *Phys. Rev. E* **79,** 021501 (2009).
11. Martin, J. E., Venturini, E., Gulley, G. L. & Williamson, J. Using triaxial magnetic fields to create high susceptibility particle composites. *Phys. Rev. E* **69,** 021508 (2004).

©2012 Macmillan Publishers Limited. All rights reserved

12. Kiss, I. Z., Zhai, Y. & Hudson, J. L. Emerging coherence in a population of chemical oscillators. *Science* **296,** 1676–1678 (2002).
13. Kantorovich, S., Weeber, R., Cerda, J. J. & Holm, C. Ferrofluids with shifted dipoles: ground state structures. *Soft Matter* **7,** 5217–5227 (2011).
14. Chen, Q. *et al.* Supracolloidal reaction kinetics of Janus spheres. *Science* **331,** 199–202 (2011).
15. Zerrouki, D., Baudry, J., Pine, D., Chaikin, P. & Bibette, J. Chiral colloidal clusters. *Nature* **455,** 380–382 (2008).
16. Erickson, R. O. Tubular packing of spheres in biological fine structures. *Science* **181,** 705–716 (1973).
17. Lohr, M. A. *et al.* Helical packings and phase transformations of soft spheres in cylinders. *Phys. Rev. E* **81,** 040401(R) (2010).
18. Riedel, I. H., Kruse, K. & Howard, J. A self-organized vortex array of hydrodynamically entrained sperm cells. *Science* **309,** 300–303 (2005).
19. Kotar, J. *et al.* Hydrodynamic synchronization of colloidal oscillators. *Proc. Natl Acad. Sci. USA* **107,** 7669–7673 (2010).
20. Adler, R. A study of locking phenomena in oscillators. *Proc. Inst. Radio Engineers* **34,** 351–357 (1946).
21. Polin, M., Tuval, I., Drescher, K., Gollub, J. P. & Goldstein, R. E. Chlamydomonas swims with two ''gears'' in a eukaryotic version of run-and-tumble locomotion. *Science* **325,** 487–490 (2009).
22. Albrecht, M. *et al.* Magnetic multilayers on nanospheres. *Nature Mater.* **4,** 203–206 (2005).
23. Duncanson, W. J. *et al.* Microfluidic synthesis of advanced microparticles for encapsulation and controlled release. *Lab Chip* **12,** 2135–2145 (2012).
24. Vilfan, M. *et al.* Self-assembled artificial cilia. *Proc. Natl Acad. Sci. USA* **107,** 1844–1847 (2010).
25. Yellen, B. B., Hovorka, O. & Friedman, G. Arranging matter by magnetic nanoparticle assemblers. *Proc. Natl Acad. Sci. USA* **102,** 8860–8864 (2005).
26. Damasceno, P. F., Engel, M. & Glotzer, S. C. Predictive self-assembly of polyhedra into complex structures. *Science* **337,** 453–457 (2012).
27. Sacanna, S., Irvine, W. T. M., Chaikin, P. M. & Pine, D. J. Lock and key colloids. *Nature* **464,** 575–578 (2010).
28. Gerbode, S. J. *et al.* Glassy dislocation dynamics in 2D colloidal dimer crystals. *Phys. Rev. Lett.* **105,** 078301 (2010).
29. Vissers, T., van Blaaderen, A. & Imhof, A. Band formation in mixtures of oppositely charged colloids driven by an ac electric field. *Phys. Rev. Lett.* **106,** 228303 (2011).
30. Jäger, S. & Klapp, S. H. L. Pattern formation of dipolar colloids in rotating fields: layering and synchronization. *Soft Matter* **7,** 6606–6616 (2011).

Supplementary Information is available in the online version of the paper.

Acknowledgements This work was supported by the US Army Research Office, grant award number W911NF-10-1-0518 (Y.J., S.C.B. and S.G.) and by the National Science Foundation under award number DMR-1006430 (M.B. and E.L.). The methods of Janus particle fabrication were supported by the US Department of Energy, Division of Materials Science, under award number DE-FG02-07ER46471 through the Frederick Seitz Materials Research Laboratory at the University of Illinois at Urbana-Champaign. We acknowledge support from the National Science Foundation, CBET-0853737 for equipment and from the Quest high-performance computing facility at Northwestern University. We thank J. Whitmer for writing the original version of the simulation code.

Author Contributions J.Y. and S.G. initiated this work. J.Y. and S.C.B. built the set-up; J.Y. performed the experiments; M.B. and E.L. performed the modelling and simulations. J.Y., M.B., E.L. and S.G. wrote the paper.

Author Information Reprints and permissions information is available at www.nature.com/reprints. The authors declare no competing financial interests. Readers are welcome to comment on the online version of the paper. Correspondence and requests for materials should be addressed to E.L. (luijten@northwestern.edu) or S.G. (sgranick@uiuc.edu).

©2012 Macmillan Publishers Limited. All rights reserved

METHODS

Particle synthesis. Onto a planar submonolayer[14] of monodisperse 3-μm silica particles (Tokuyama), an 18-nm or 21-nm nickel coating followed by a SiO_2 coating 15–20 nm thick is deposited vertically using electron-beam deposition. The SiO_2 layer prevents oxidation of nickel and makes the particle chemically isotropic. A control glass slide without particles is coated simultaneously and used to measure the apparent film thickness by ellipsometry (J. A. Woollam VASE ellipsometer). Magnetic hysteresis-loop measurements are performed using a SQUID magnetometer (Quantum Design MPMS-XL) on a dense monolayer of particles (0.5 cm × 0.5 cm). The monolayer is washed thoroughly with deionized water and isopropyl alcohol, then sonicated in water to collect the particles. In deionized water, the particles have a ζ potential of -36 ± 6 mV (Malvern Zetasizer Nano).

Set-up. A spatially homogeneous precessing magnetic field is generated by three orthogonal pairs of solenoids (Science Source 14835 with iron cores, and custom-designed coils from Teachspin) in a home-built magnetic set-up. Two pairs of solenoids receive two sinusoidal voltages from a function generator (Agilent 33522A), amplified by power amplifiers (Kepco 100-4D), with $\pi/2$ phase difference between each signal to produce the rotating component of the precessing field. The third pair of solenoids is connected to a direct-current power supply (Hewlett-Packard 6266B), to provide the static component of the precessing field. The field strength and frequency response are calibrated using a triaxial Gaussmeter (Alpha Lab Model VGM). The magnetic field is homogeneous within 5% across 1 cm, which greatly exceeds the maximum field of view of 170 μm × 128 μm. Videos are taken in a home-built microscope using an LED light source (Thorlabs MCWHL2), a 50× long-working-distance objective (Mitutoyo, numerical aperture 0.55) and a CMOS camera (Edmund Optics 5012M GigE).

Single-particle tracking. A dilute suspension ($\sim 10^{-2}$ mg ml^{-1}) of Janus particles in deionized water is introduced into the imaging chamber (Lab-Tek II chambered cover glass). The particles sediment to the bottom, but negative charges on the silica particles prevent adsorption to the chamber walls as well as irreversible clustering of particles. A precessing magnetic field is applied with precession axis either perpendicular or parallel to the bottom wall; in the parallel case the particles roll on the wall and translate accordingly. By restricting the field of view to a small area, we capture high-speed videos of single-particle dynamics at ~600 frames per second. The rotation and oscillation frequencies of the particles are determined using home-written Matlab code. For each θ, at least five particles are analysed. Standard deviations are smaller than the symbols in Fig. 1b.

Equations of motion. The full derivation and discussion are given in the Supplementary Information. In summary, by treating each particle as a paramagnetic sphere with an anisotropic susceptibility tensor, and balancing the magnetic torque by the viscous torque by assuming an overdamped condition[10], we arrive at two coupled differential equations:

$$\frac{d\alpha}{dt} = \omega_c(\sin\alpha\cos\beta\sin\theta - \cos\alpha\cos\theta)(\cos\alpha\cos\beta\sin\theta + \sin\alpha\cos\theta)$$

$$\frac{d\beta}{dt} = \omega_H + \omega_c\frac{\sin\beta\sin\theta}{\cos\alpha}(\cos\alpha\cos\beta\sin\theta + \sin\alpha\cos\theta)$$

in which ω_H is the field frequency and φ and α are the azimuth angle and the complement of the inclination angle of the particle director defined in Supplementary Fig. 4, respectively. The parameter $\beta = \omega_H t - \varphi$ is the phase lag between the azimuth angles of the external field and the particle, and ω_c is defined as $\mu_{water}V_{Ni}\Delta\chi H^2/\zeta_r$, a characteristic frequency arising when magnetic force and viscous force are balanced. μ_{water} is the permeability of the medium, V_{Ni} is the volume of magnetic material on a single particle, ζ_r is the rotational drag coefficient, and $\Delta\chi = \chi_\perp - \chi_{||}$, where $\chi_{||}$ is the susceptibility parallel to the Janus director $\hat{n}$ and $\chi_\perp$ is the susceptibility in any direction perpendicular to $\hat{n}$. For example, the case of 18-nm Ni coating and 5-mT field strength yields $\omega_c = 942$ rad s^{-1}, corresponding to 150 Hz. We use this value and the equations of motion to predict the rotation/oscillation frequencies presented in Fig. 1b.

Protocol for applying the magnetic field. Before each experiment, particles are concentrated on one side of the cell using a 20-Hz, 5-mT rotating field that drives the particles towards one side of the imaging chamber. Subsequently a precessing field with opposite direction of rotation is applied with the precession axis parallel to the bottom of the sample cell (horizontal or vertical in the images). Videos are taken at rates of up to 300 frames per second for individual structures. Within 5 min, microtubes form and their distribution reaches a steady state within 10 min. We image the middle of the cell, covering a broad range of concentrations where individual tubes exist with minimum mutual interference. The distribution is quantified by visual inspection of the structures; rotation exposes different faces of the tubes, facilitating their determination. Over 3,000 particles are included in each sample. For each θ, at least four independent samples are analysed. Error bars in Fig. 2c correspond to one standard deviation.

Simulation. Molecular dynamics computer simulations are performed with self-consistent magnetic interactions and shifted-truncated Lennard–Jones interactions at field strength and frequency equivalent to 5 mT and 20 Hz, for 2×10^8 time steps. The system has dimensions $40 \times 40 \times 80$ or $40 \times 40 \times 160$ in reduced simulation units and contains up to 80 particles; doubling the system size confirms the same trends. The colloid diameter in these units is 4.3. The time step of 0.001 ($\approx 1.26 \times 10^{-7}$ s) provides energy stability in the overdamped regime where we operate. Each particle is treated as a sphere with a point dipole shifted from the particle's geometric centre. The anisotropic magnetic susceptibility is scaled by the experimental hysteresis curve and the dipole–moment shift is determined by matching the experimentally observed bond angle of the zigzag chain in a static magnetic field. Magnetic interactions are determined at each time step by solving the linear system of equations for each particle's magnetic moment as a function of the field produced by the other particles and the spatially uniform, time-dependent external field. Simulations to evaluate microtube structure stability begin with particles arranged in the given structure, at the equilibrium pair distance, with particles oriented towards the microtube's central axis. Particles relax into their steady-state configuration provided that the structure is stable for the given parameters. S is defined as $\frac{1}{n}\left|\sum_{j=1}^{n}\exp(i2k\theta_{jin})\right|$, where θ_{jin} is the azimuth angle of a particle j's position vector (Supplementary Fig. 8).

©2012 Macmillan Publishers Limited. All rights reserved